JOURNAL OF GUIDANCE, CONTROL, AND DYNAMICS
Vol. 16, No. 6, November–December 1993

Six-Degree-of-Freedom Guidance and Control Analysis of Mars Aerocapture

Richard W. Powell* and Robert D. Braun*
NASA Langley Research Center, Hampton, Virginia 23681

A six-degree-of-freedom (6DOF) simulation has been developed to investigate the control and guidance issues of a Mars aerobraking vehicle. The guidance algorithm used is a predictor-corrector guidance formulation designed to control the exit orbital apoapsis and wedge angle using bank angle modulation. Major features of this predictor-corrector guidance algorithm include 1) integration of the 3DOF equations of motion within an inner-loop simulation, 2) load-relief logic, 3) finite roll rates, and 4) an aerodynamic feedback multiplier. The algorithm has been shown to be capable of successfully guiding the vehicle through combinations of atmospheric density dispersions, aerodynamic mispredictions, and off-nominal atmospheric interface conditions. This study demonstrated that the addition of vehicle dynamics to the Mars aerobraking simulation does not significantly impact mission feasibility. That is, a good control system design coupled with an adaptive guidance algorithm can ensure mission success (as measured by the required postaerocapture propulsive maneuvers) in the presence of numerous off-nominal conditions.

Nomenclature

A = density variation amplitude
C_D = drag coefficient
$C_{D_{nom}}$ = nominal drag coefficient
C_L = lift coefficient
$C_{L_{nom}}$ = nominal lift coefficient
E = energy, m^2/s^2
e = eccentricity
g = gravitational acceleration at Earth's surface (9.806 m/s^2)
I_{sp} = specific impulse, s
i = inclination, deg
LH_2 = liquid hydrogen
LOX = liquid oxygen
p = roll rate, deg/s
q = pitch rate, deg/s
r_s = stability axis yaw rate, deg/s
S = aerobrake surface area, m^2
U_{x_c} = number of commanded roll RCS thrusters
U_{y_c} = number of commanded pitch RCS thrusters
U_{z_c} = number of commanded yaw RCS thrusters
V_{atm} = atmospheric interface velocity, km/s
w = horizontal density variational wavelength, km
y = downrange distance, km
α = angle of attack, deg
α_{error} = angle-of-attack error, deg
β = sideslip angle, deg
γ_{atm} = atmospheric interface flight path angle, deg
ΔV = propulsive velocity change, m/s
ρ = atmospheric density, kg/m^3
ρ_{mean} = mean atmospheric density
ϕ = bank angle, deg
ϕ_c = commanded bank angle, deg
ϕ_{error} = bank-angle error, deg
ω = wedge angle, difference between target and actual angular momentum vectors, deg
Ω = longitude of ascending node, deg

Presented as Paper 92-0736 at the AIAA 30th Aerospace Sciences Meeting, Reno, NV, Jan. 6-9, 1992; received Feb. 18, 1992; revision received Jan. 25, 1993; accepted for publication Feb. 8, 1993.

*Aerospace Engineer, Space Systems Division. Member AIAA.

Introduction

WITH renewed interest in manned lunar and planetary exploration, NASA is presently analyzing the aspects of a manned mission to Mars in the early twenty-first century. For the first manned flights, a chemical-rocket system is one of the leading propulsion candidates. Because of the high transportation costs of launching to low-Earth orbit (LEO), much of the mission feasibility hinges on minimizing the initial LEO weight. One method for reducing the initial LEO weight requirements is to employ aerobraking to decelerate the spacecraft upon Mars arrival and Earth return. In comparison with an all-propulsive chemically propelled vehicle, aerobraking upon Mars arrival and Earth return has been shown to yield an initial mass reduction of 20–60%.[1]

Aerobraking is defined as the deceleration resulting from the effects of atmospheric drag upon a vehicle; thus, aerobraking eliminates the retro-propulsion requirements for orbital capture, greatly reducing the amount of required propellant. For an interplanetary mission that uses aerobraking, entry performance analyses are required to ensure that precisely enough energy is dissipated so that the vehicle transitions from its hyperbolic entry path to the desired parking orbit about the target planet without exceeding any constraints (e.g., maximum deceleration). Entry performance analyses are also performed to evaluate the effect of uncertainties upon the mission profile. At Mars arrival, a majority of this uncertainty can be attributed to atmospheric interface errors (resulting from interplanetary navigation limitations) as well as to atmospheric density and vehicle aerodynamic mispredictions. Therefore, in any mission scenario that includes aerobraking, atmospheric as well as interplanetary issues must be considered in the design of an optimum transfer vehicle.

Many guidance algorithms have been proposed for Mars aerocapture.[2-4] These guidance algorithms range from adaptations of Apollo and Space Shuttle entry guidance algorithms to those that calculate the current optimal trajectory based on sensed conditions using onboard computers. The algorithms developed for entry vehicles to date have developed desired reference profiles to which the vehicle has been commanded to fly.[5,6] These algorithms are vehicle specific and in general do not provide full coverage of the theoretical performance footprint. With the advances in computer technology, it is currently possible to develop guidance algorithms that are adaptable to a range of vehicles with minimal modification and allow for fuller use of the theoretical performance limits.[2] Three guidance algorithms were recently evaluated using 3DOF simulations in support of the proposed Aeroassist

Flight Experiment.[7] Two of these algorithms relied on predictor-corrector logic for the atmospheric pass.

This paper further examines a predictor-corrector algorithm[8] using a 6DOF simulation. This 6DOF evaluation was performed to assess the impact of vehicle dynamics on mission feasibility. The algorithm is responsible for guiding the vehicle through the Martian atmosphere in the presence of off-nominal conditions to the desired conditions at atmospheric exit. The off-nominal conditions simulated include 1) errors in the atmospheric interface conditions, 2) atmospheric density variations (vertical and horizontal), and 3) misprediction of the vehicle's aerodynamic characteristics. The effect of multiple off-nominal conditions was also evaluated. Additionally, the algorithm is used to limit the maximum deceleration level through bank angle modulation. For this investigation, a control system was designed, the predictor-corrector guidance algorithm was implemented, and 6DOF simulations were conducted using off-nominal conditions similar to those in Ref. 8.

Mission

The aerobrake is designed to transition the vehicle from its interplanetary approach trajectory to a captured parking orbit about Mars. The desired parking orbit for this analysis is a highly elliptical orbit (250 × 33,786 km) with a period of one Martian day (24.6 h). Because the conditions at the atmospheric interface are dependent on the launch date, the vehicle must be designed to handle a range of interface conditions. However, Ref. 9 has shown that interplanetary trajectory shaping can be used to satisfy a prescribed range of atmospheric interface conditions, while still offering a large number of launch opportunities (with only a small increase in required propellant). Therefore, this study considered entry velocities between 6 and 8 km/s as being adequate to provide sufficient launch opportunities. This study concentrated on a low lift-to-drag ratio (L/D) vehicle to stress the guidance algorithm.

Upon completion of the aerocapture maneuver, propulsive burns are performed first at apoapsis (primarily to raise the periapsis out of the atmosphere), then at the periapsis (primarily to adjust for apoapsis error as a result of the off-nominal conditions), and finally at the crossing of the actual orbit and target orbit planes nearest apoapsis (primarily to eliminate any remaining wedge angle). While this sequence of burns may not produce the absolute minimum ΔV, it does provide comparative results. The velocity increment required to accomplish these three maneuvers is used as a figure of merit in evaluating mission success. Note that the ΔV associated with the reaction control system (RCS) thruster firings during the atmospheric pass are not included in the figure of merit. Nominal atmospheric exit conditions are specified in terms of the Mars parking orbit energy (which specifies the semimajor axis), eccentricity (which is used to specify periapsis altitude), inclination, and longitude of the ascending node. Specification of the argument of periapsis is not performed in this analysis.

Vehicle Description

The vehicle that was used in this study consists of the aerobrake, its associated structure, and a payload. The payload was assumed to consist of three habitation modules, a Mars excursion module (MEM), Mars departure propellant and tankage, and an Earth-return capsule. The habitation modules, which are adapted from space station hardware, provide approximately 300 m^3 of living space. The MEM includes all of the vehicle components that are used in the descent to, exploration of, and ascent from the Martian surface. The liquid oxygen/hydrogen propulsion system has an I_{sp} of 480 s and was sized to provide the representative Mars departure burn of 1.7 km/s. Earth-return deceleration is accomplished with a crew capsule based on the Apollo capsule shape. Note that in this analysis, the Mars aerobrake and associated structure is assumed to be 15% of the mass that is aerobraked. Of the various possible aerobrake configurations, an enlarged version of the Aeroassist Flight Experiment[10] was selected because of the available aerodynamic data base. The Mars entry configuration is shown in Fig. 1. Note that all the payload elements are packaged within the subsonic wake region denoted by the rays emanating from the aerobrake and converging at a point behind the vehicle. The aerodynamics used were those presented in Ref. 11. At the nominal trim angle of attack of 17 deg, this configuration has an L/D of 0.28. This vehicle is controlled by an RCS that provides three-axis control moments. The RCS thrusters are assumed to be located on the rim of the aerobrake and to produce pure couples. To date, no wind tunnel or computational fluid dynamics analysis has been performed to confirm this assumption. Each RCS control thruster produces a moment 160,000 N-m. The number of thrusters that can be commanded about each axis is either 1 or 2 for yaw, and 2 or 4 for pitch and roll. A more detailed discussion of several vehicle design issues can be found in Ref. 12, which includes the packaging requirements that insure the proper location of the center of gravity.

Flight Control System

A flight control system was designed assuming all the controlling moments are provided by the RCS. The control system was initially designed using a computer program known as Interactive Digikon,[13] and then this control system was refined using the 6DOF version of the Program to Optimize Simulated Trajectories (6DPOST).[14] For this analysis, the control system design was developed as a continuous system and converted to an equivalent discrete system within the 6DPOST simulation using the convolution technique. Digikon was used to design

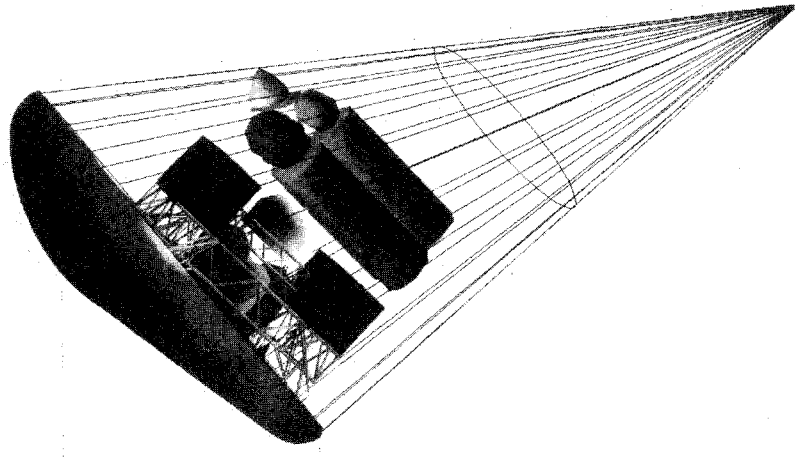

Fig. 1 Mars aerocapture configuration.

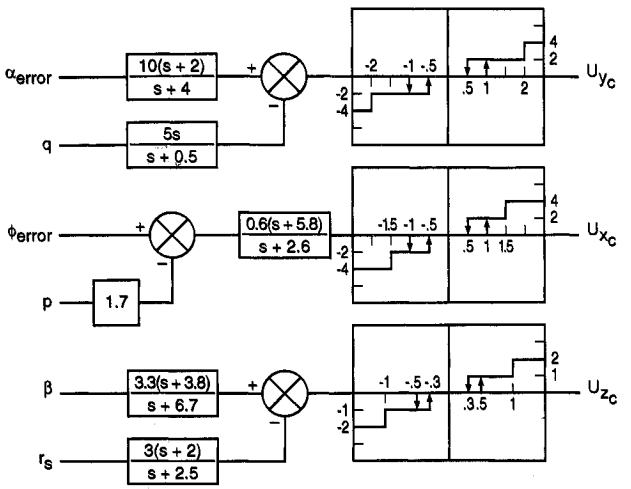

Fig. 2 Flight control system.

the control system using linearized, decoupled pitch and roll/yaw dynamics. This control system was implemented into 6DPOST, where the control system was refined by using coupled nonlinear equations. This was done by requiring the vehicle to fly a double triangular wave profile (either pitch or roll) within a specified tolerance. 6DPOST varied the control parameters (filter constants and gains) to fly this profile within the specified tolerance while minimizing RCS fuel consumption. Figure 2 shows the flight control system. Note that the control system, as designed, requires no gain scheduling. The control laws and RCS system were designed to provide a maximum roll acceleration of 5 deg/s^2, a maximum roll rate p of 20 deg/s, maintain sideslip angle β between $\pm$ 1 deg, and angle of attack α between 16.8 and 17.2 deg. The U_{y_c} command logic is driven by the angle-of-attack error ($\alpha_c - \alpha_{nom}$) with the q feedback. The U_{y_c} can be either 2 or 4 thrusters depending on the driving error signal. The U_{x_c} command logic is driven by the bank angle error signal ($\phi_c - \phi$) with the ρ feedback. The U_{x_c} can be either 2 or 4 thrusters depending on the driving error signal. The U_{z_c} command logic is driven by the β angle with r_s feedback. The U_{z_c} can be either 1 or 2 thrusters depending on the driving error signal. To prevent control system ringing, all signals are processed through hysteresis filters.

Guidance Algorithm

The guidance algorithm used in this analysis employs a predictor-corrector technique. Conceptually, this algorithm determines the path required to direct the vehicle from its current state to the proper exit state in the presence of off-nominal conditions. The trajectories evaluated were simulated with the 6DOF version of the 6DPOST.[14] The predictor-corrector guidance capability was implemented by including a 3DOF simulation as an inner loop to the main simulation. In this manner, the predictor-corrector guidance model uses nominal environmental characteristics (e.g., planet, atmosphere, gravity, aerodynamic, propulsion, and weights), whereas the main simulation may include perturbed characteristics. For the present study, identical simulation models, with the exception of the Mars atmosphere and vehicle aerodynamics, were used by both the main simulation and the predictor-corrector guidance algorithm. Hence, the effects of atmospheric uncertainty and aerodynamic characteristic mispredictions can be singled out for evaluation.

The predictor-corrector algorithm is called by an outer-loop guidance routine at specified time intervals throughout the atmospheric passage. Upon atmospheric entry (atmospheric interface assumed to be 300 km), the guidance algorithm first determines the constant-bank-angle and roll reversal history that would result in the proper exit energy with 2-deg or less wedge angle. The predictor-corrector algorithm first numerically integrates the 3DOF translational equations about a spherical rotating planet using the bank angle determined from the previous call to the algorithm, or the default value for the first call. Based on the exit apoapsis condition, the direction of search for the correct bank angle is determined. Once the direction of search is obtained, the required bank angle is found by using one-dimensional search logic. If the search logic cannot find the bank angle required to reach the proper exit conditions, the vehicle is commanded to roll either full lift up, or full lift down, the direction determined to minimize the exit error. In the present study, this situation was only found to occur near the end of the atmospheric pass (where the ability to control the exit conditions is small because of low dynamic pressure over the remaining portion of the trajectory). If the peak deceleration level encountered using this bank angle exceeds the design limits, the deceleration or load-relief logic is implemented.

For this manned mission, the maximum deceleration was specified as 5 g. If the constant-bank-angle atmospheric transfer does not exceed the 5-g deceleration limit, no load relief is required. However, if the deceleration constraint is exceeded, a one-dimensional search technique is used to determine the bank angle that would result in a 5-g maximum deceleration. Once the peak deceleration level is reached in the outer-loop simulation, the algorithm reverts to determining the roll angle history that results in the proper atmospheric exit energy and wedge angle. A more detailed discussion of the ability of bank-angle modulation to provide load relief is found in Ref. 8.

To improve the performance of the predictor-corrector algorithm, an aerodynamic feedback multiplier is included. This multiplier on the nominal density profile is used by the predictor-corrector algorithm so that the inner-loop drag force matches the actual drag force each time the predictor-corrector algorithm is invoked. In the current formulation no filtering of the actual drag force is used. Utilization of this factor is analogous to the use of onboard accelerometer measurements during flight. In this manner, a density bias throughout the entire profile will not degrade performance.

Two major differences exist between the guidance algorithm used in the 6DOF simulations and the algorithm described in Ref. 8. The first is that the load-relief logic has been changed to produce a bank-angle history such that the specified deceleration limit is achieved (even in the presence of atmospheric density variations). In this manner, proper energy control is enhanced. Once the maximum deceleration point is passed, the vehicle rolls to the bank angle required to produce the proper atmospheric exit conditions. In the earlier work, the vehicle initially flew a bank angle history that would result in the correct orbital exit energy, and fully unroll (lift vector up) prior to maximum deceleration to avoid exceeding the limit. In the previous study, time to unroll was determined by the predictor-corrector guidance algorithm. With the inclusion of vehicle dynamics, the time required to perform this roll maneuver was determined. These dynamic models showed that the time required to unroll and then roll to the proper bank angle after maximum deceleration was excessive, and would increase the sensitivity of the vehicle to off-nominal density profiles. For the present study, this maneuver was modified so that the vehicle would fly the roll angle that resulted in the maximum allowable deceleration when load-relief logic is required. The second difference is that the fidelity of the inner-loop 3DOF predictor-corrector equations of motion were enhanced to include finite roll rates and accelerations. It was found that if these enhancements were not made, the energy dissipated during the roll reversals was not calculated, and large errors in exit energy could result.

Results and Discussion

The significance of various mission uncertainties can be assessed with a guided atmospheric simulation. In this section,

several types of dispersions are simulated and discussed. These off-nominal conditions include 1) atmospheric density variations, 2) aerodynamic characteristic mispredictions, and 3) off-optimum entry flight path angle. In the present study, each of the effects is first evaluated individually to gain an understanding of its impact on mission success. Then the off-nominal conditions are simulated in combinations.

Nominal Trajectory

The nominal atmospheric pass of the aerobrake with a 6 km/s V_{atm} is shown in Fig. 3. For the nominal case the vehicle flies at an ϕ of approximately -110 deg until the wedge angle ω exceeds -2 deg. At this time the vehicle is commanded to perform a roll reversal to reduce ω. Note that α remains within 0.2 deg of the commanded value (α_c) of 17 deg, and β remains within ± 1 deg. The postaerocapture ΔV required to place the vehicle in the desired parking orbit is 18 m/s.

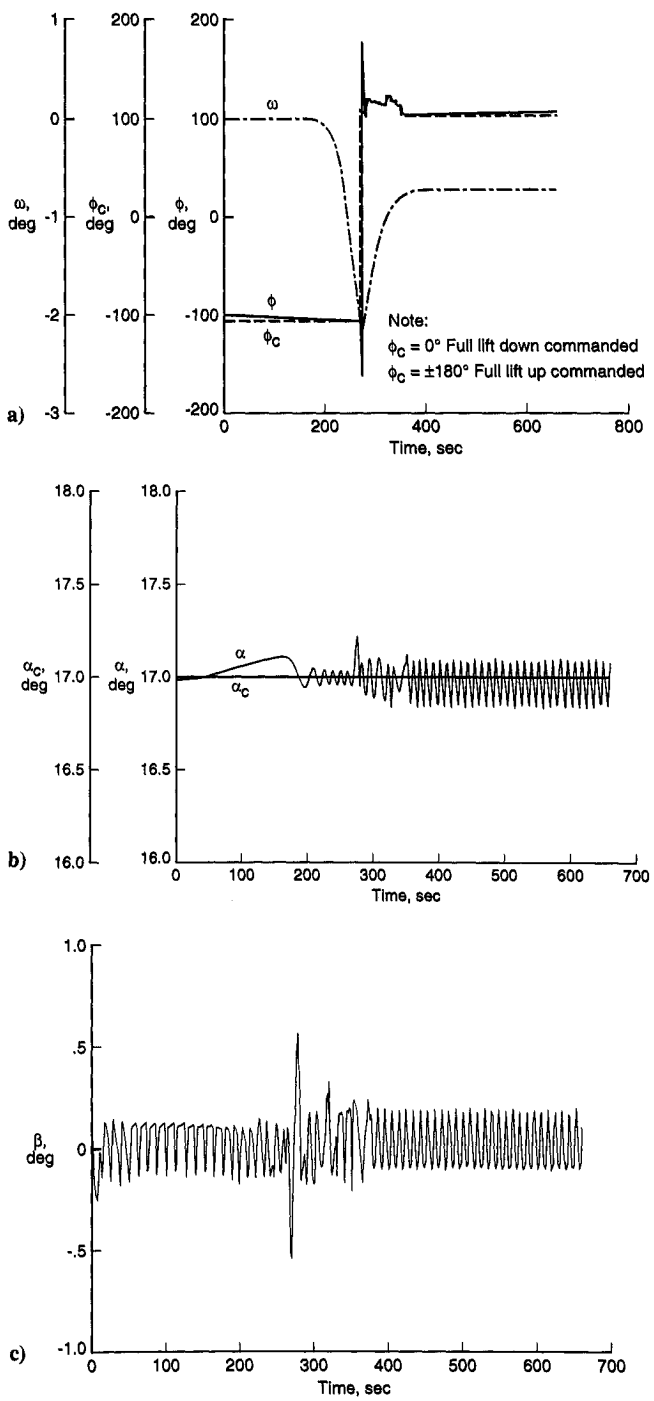

Fig. 3 Nominal aerobraking trajectory: a) ω, ϕ_c, ϕ time histories; b) α_c, α time histories; and c) β time history.

Atmospheric Density Variations

To evaluate the significance of various levels of atmospheric density uncertainty on the guidance algorithm, two atmospheric density profiles must be provided to the simulation. One profile must be used in the guidance, or inner-loop simulation (the predicted or expected density profile), and the other used in the outer-loop simulation (the encountered density profile). Figure 4 illustrates twelve randomly generated Mars atmospheric density profiles. These profiles (a few of which include the density effects of local dust storms) were generated by the Mars-GRAM program.[15] These random profiles were used in the outer-loop simulation (the encountered density profile), whereas the mean density profile was used in the inner-loop simulation as the expected density profile. High- and low-density profiles, which bound the random profiles, were also generated. These extreme profiles are shown by the dashed lines in Fig. 4. Mars aerobraking trajectories were then simulated for each random and extreme profile with entry and exit conditions as listed in Table 1. Note that the initial and final orbital planes are coincident, which results in mandatory roll reversals for every simulation to control wedge angle. This was done intentionally to stress the guidance and control algorithms. In an operational scenario, the vehicle could enter at some predetermined offset angle to reduce or eliminate the roll reversals.

To compensate for an atmospheric density profile different from the expected, the guidance algorithm commands a series of roll maneuvers, which are illustrated in Fig. 5. Note that the roll maneuvers shown are for the two extreme density profiles; for comparison, the nominal roll history in which the mean density profile was utilized is also shown. Altitude and energy

Table 1 Simulation initial and target conditions

Initial Conditions		
V_{atm}, km/s	6	8
γ_{atm}, deg	−17.84	−19.73
Altitude, km	300	300
E, km^2/s^2	6.415	20.415
e	2.03	4.27
i, deg	30.0	30.0
Ω, deg	0	0
Target Conditions		
Apoapsis, km	33,786	33,786
Periapsis, km	250	250
e	0.82	0.82
i, deg	30.0	30.0
Ω, deg	0	0

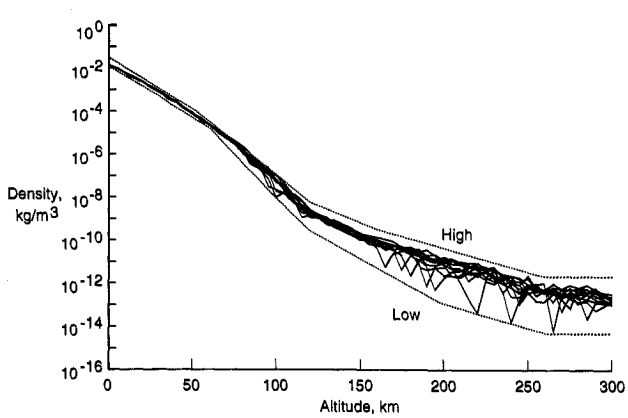

Fig. 4 Mars-GRAM generated atmospheric density profiles.

loss histories are shown in Fig. 6. Note that, although different flight profiles are followed, the appropriate energy decrement is achieved regardless of the density profile. Hence, the guidance algorithm is able to compensate for either of the two extreme density profiles with bank-angle modulation so that the proper exit energy conditions are met.

From a mission feasibility standpoint, the severity of unexpectedly encountering one of the random or extreme density profiles can be assessed by considering the required increase in the amount of postaerocapture ΔV. Based on the results of Fig. 6, a relatively minor ΔV penalty is expected. Fig. 7 depicts the required ΔV for missions in which each of these unexpected density profiles were encountered. For comparison purposes, the nominal postaerocapture ΔV is also shown. This figure shows that only a minor increase in postaerocapture ΔV is required to account for the uncertainty in these density models (the greatest increase was 6.3 m/s for a V_{atm} of 6 km/s, and 8 m/s for a V_{atm} of 8 km/s).

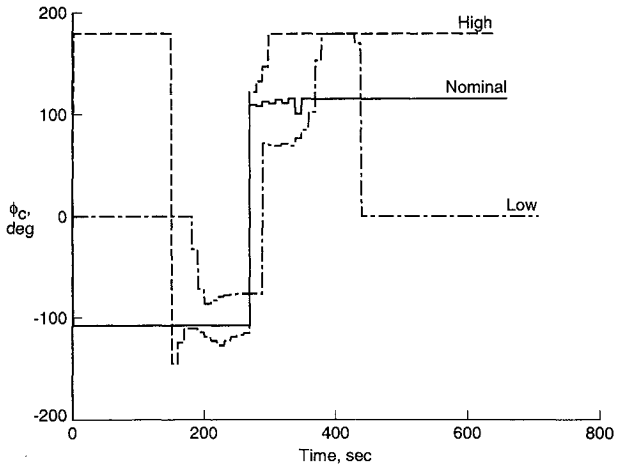

Fig. 5 Bank angle profiles resulting from unexpected density profiles (V_{atm} = 6 km/s).

The previous discussion of density dispersions focused on the use of vertical variations in the atmospheric density profile; that is, the density variation was assumed to be a function of altitude. However, recent research has focused interest on the effects of horizontal density variations; that is, density variations along the flight path at a fixed altitude. Horizontal variations are believed to be present in the Martian atmosphere and are generally simulated by using either a sinusoidal wave or step function. In this analysis, these dispersions were simulated with a sinusoidal wave equation of the form

$$\rho = \rho_{mean}\left\{1.0 + A\left[\sin(2\pi y/w + \pi/4)\right]\right\}$$

This equation was used to vary the encountered density (outer-loop value) profile in a wave-like manner. An amplitude of 0.3 was used, and wavelengths of 50, 500, and 5000 km were investigated for a nominal aerobraking trajectory with entry and exit conditions as listed in Table 2. By using a range of wavelengths, the effects of both density shears (small wavelengths) and density shifts (large wavelengths) were investigated. Figure 8 shows the two extremes of the density profiles encountered (wavelengths of 50 and 5000 km) and the corresponding bank angle histories. Note that, although the amplitude of the sinusoidal wave is fixed, the dispersion increases in

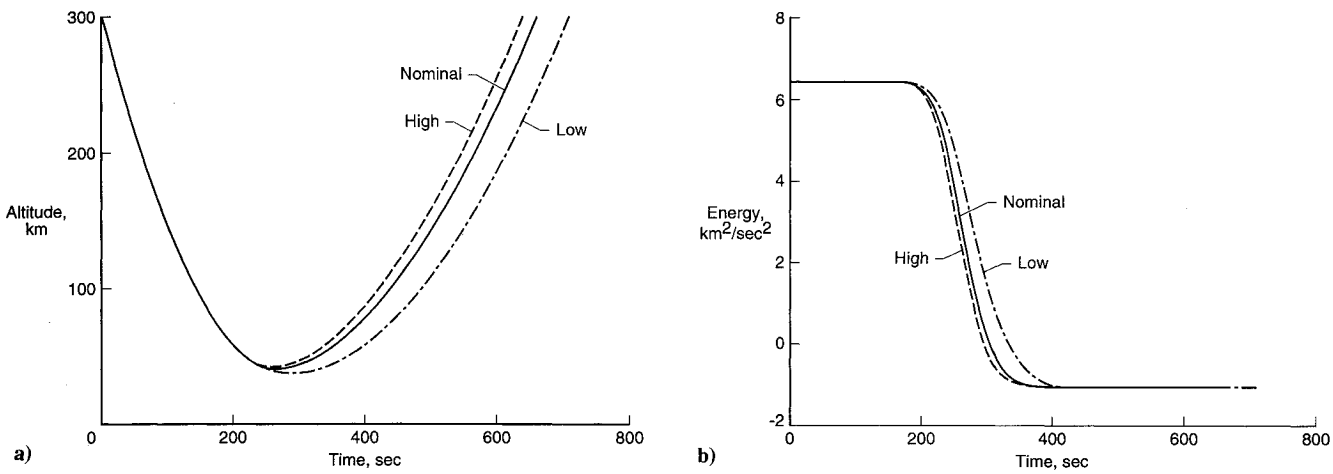

Fig. 6 Altitude and orbital energy profiles resulting from unexpected density profiles (V_{atm} = 6 km/s): a) altitude and b) orbital energy.

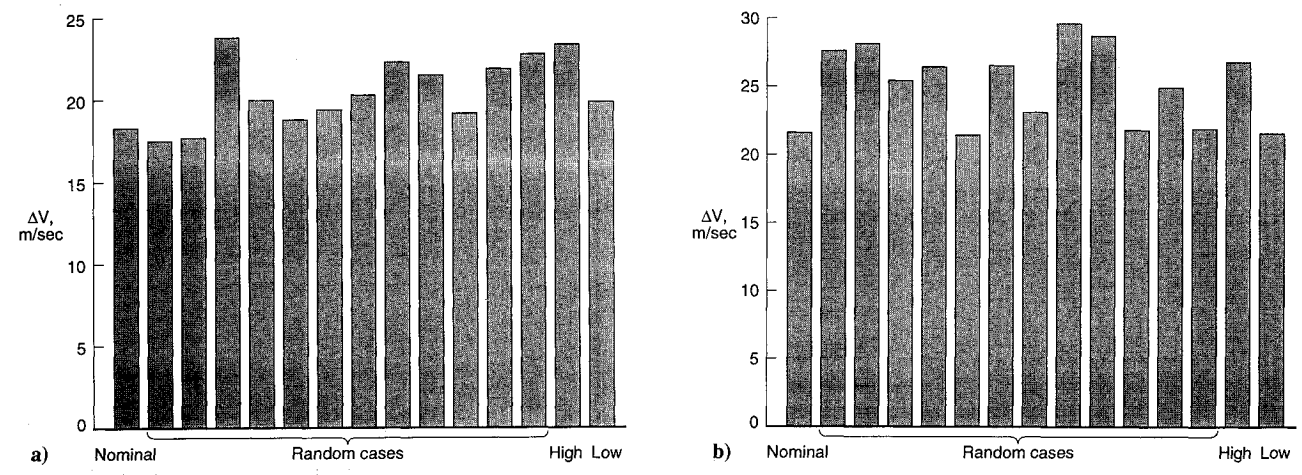

Fig. 7 Postaerocapture ΔV requirements resulting from unexpected density profiles: a) V_{atm} = 6 km/s and b) V_{atm} = 8 km/s.

Table 2 Postaerocapture ΔV results from multiple off-nominal conditions

$C_{L_{nom}}$ factor	$C_{D_{nom}}$ factor	γ_{atm}[a]	Atmosphere[b]	ΔV V_{atm} = 6 km/s, m/s	ΔV V_{atm} = 8 km/s, m/s
1.0	1.0	Nom	Mean	18	22
1.1	1.0	Nom − 0.1 deg	High[c]	23	32
0.9	1.0	Nom − 0.1 deg	High	26	53
1.1	1.0	Nom + 0.1 deg	High	31	22
0.9	1.0	Nom + 0.1 deg	High	29	25
1.0	1.1	Nom − 0.1 deg	High	22	70
1.0	0.9	Nom − 0.1 deg	High	26	22
1.0	1.1	Nom + 0.1 deg	High	40	25
1.0	0.9	Nom + 0.1 deg	High	37	31
1.1	1.0	Nom − 0.1 deg	Low[d]	19	26
0.9	1.0	Nom − 0.1 deg	Low	30	31
1.1	1.0	Nom + 0.1 deg	Low	30	22
0.9	1.0	Nom + 0.1 deg	Low	21	23
1.0	1.1	Nom − 0.1 deg	Low	28	51
1.0	0.9	Nom − 0.1 deg	Low	21	22
1.0	1.1	Nom + 0.1 deg	Low	21	73
1.0	0.9	Nom + 0.1 deg	Low	20	19

[a]Nom refers to nominal atmospheric interface flight path angle.
[b]Mean refers to mean atmospheric density profile.
[c]High refers to that perturbed atmosphere that resulted in highest atmospheric exit apoapsis.
[d]Low refers to that perturbed atmosphere that resulted in lowest atmospheric exit apoapsis.

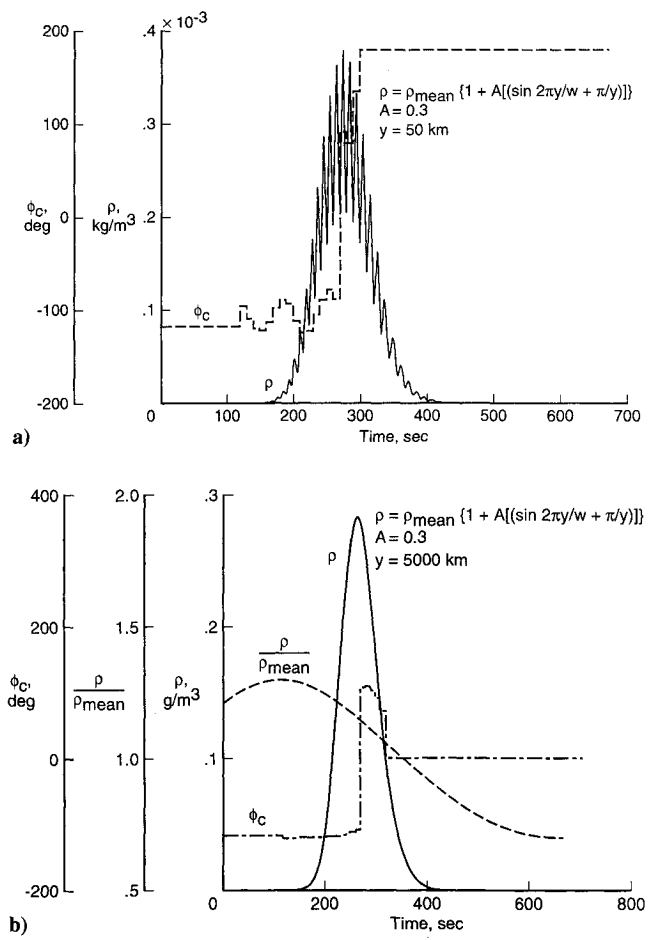

Fig. 8 Density and commanded bank angle profiles resulting from unexpected horizontal density waves (V_{atm} = 6 km/s): a) wavelength = 50 km, amplitude = 30% and b) wavelength = 5000 km, amplitude = 30%.

magnitude with decreasing altitude because the encountered density is also a function of the mean density profile without a wave. Thus, because a majority of the deceleration occurs near periapsis of the atmospheric trajectory (in the 30–50-km altitude region) where the sensed density is the largest, significant off-nominal variations are simulated with use of this equation in the critical atmospheric region. In the cases illustrated in Fig. 8, the guidance algorithm was capable of guiding the vehicle through a sinusoidal density variation of 30% with the use of bank-angle modulation for the wavelengths simulated. The severity of encountering a wave-like variation in the density profile was assessed in terms of the required increase in the amount of postaerocapture ΔV. This ΔV is shown as a function of wavelength and V_{atm} in Fig. 9. The maximum increase in this ΔV over the nominal is 132 m/s for a V_{atm} of 6 km/s, and 127 m/s for a V_{atm} of 8 km/s. These increases are for the shortest wavelength case, namely 50 km. The ΔV required for the wavelengths of 500 and 5000 km/s only show small increases over the nominal values (22 m/s for V_{atm} = 6 km/s, and 28 m/s for V_{atm} = 8 km/s). While the ΔV are much larger for the short-wavelength horizontal density waves than for the vertical dispersions, the ΔV remain within reasonable limits. Additionally, this ΔV could be reduced through the addition of density filtering techniques.

Aerodynamic Characteristic Mispredictions

Historically, one issue that has plagued entry vehicle design is the inability to accurately predict aerodynamic characteristics of the entry vehicle. A majority of the Mars aerobraking concepts presently under study do not have aerodynamic control surfaces. Instead, these concepts generally fly at the trim angle of attack and rely on a reaction control system to achieve the proper roll orientation. Hence, a reliable set of predicted nominal and off-nominal aerodynamic characteristics is vital to mission success. Additionally, the vehicle's onboard guidance algorithm must be capable of guiding the aerobrake through the Martian atmosphere under the influence of a mispredicted set of vehicle aerodynamics. In this analysis, the effect of a ± 10% error in C_L and C_D are evaluated. The maximum increase in ΔV over the nominal is 8 m/s for a V_{atm} of 6 km/s, and 13 m/s for a V_{atm} of 8 km/s. Further discussion of the impact of aerodynamic characteristics mispredictions can be found in Ref. 12.

Off-Nominal Atmospheric Interface Conditions

Because of the uncertainty in the interplanetary navigation, the vehicle may not encounter the atmospheric interface at the optimum conditions. To simulate atmospheric interface errors, the γ_{atm} was varied by ± 0.1 deg at the assumed atmospheric interface of 300 km. Recent studies have shown that the achievable encounter navigation error in terms of flight path angle could be less than ± 0.1 deg at 125 km with either fast turnaround Earth-based tracking, vehicle onboard optical, or vehicle ranging to an existing Mars orbiter.[16] This error bound at 125 km equates to a larger error bound of ≅ ± 0.25 deg at the 300 km atmospheric interface. Hence, the error interface condition assumed by this investigation may be larger than required. The maximum increase in ΔV over the nominal is 3 m/s for a V_{atm} of 6 km/s, and 1 m/s for a V_{atm} of 8 km/s.

Multiple Off-Nominal Conditions

In the actual flight environment, some combination of off-nominal atmospheric, aerodynamic, and initial state conditions will be encountered. Hence, combinations of off-nominal conditions were simulated. These cases combined the random atmospheric vertical density profiles that produced the largest exit apoapsis errors (highest and lowest apoapsis at atmospheric exit) with the off-nominal aerodynamics and γ_{atm} errors as described earlier. (Note that horizontal density waves were not included in these simulations because the study had demonstrated that a more detailed density filtering strategy

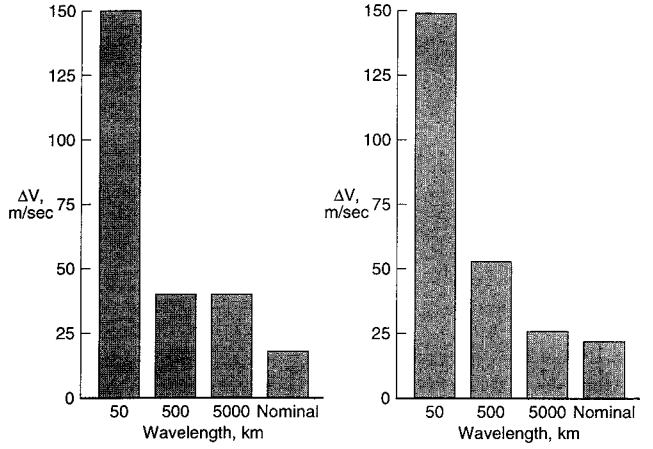

Fig. 9 Postaerocapture ΔV requirements resulting from unexpected horizontal density waves: a) $V_{atm} = 6$ km/s and b) $V_{atm} = 8$ km/s.

would be needed.) The postaerocapture ΔV required for each of these cases is shown in Table 2. The maximum increase in ΔV over the nominal is 22 m/s for a V_{atm} of 6 km/s, and 47 m/s for a V_{atm} of 8 km/s.

Summary

A 6DOF simulation has been developed to investigate the control and guidance issues of a Mars aerobraking vehicle. The guidance algorithm used is a predictor-corrector guidance formulation designed to control the exit orbital apoapsis and wedge angle using bank-angle modulation. Major features of this predictor-corrector guidance algorithm include 1) integration of the 3DOF equations of motion within an inner-loop simulation, 2) load-relief logic, 3) finite roll rates, and 4) an aerodynamic feedback multiplier. The algorithm has been shown capable of successfully guiding the vehicle through combinations of atmospheric density dispersions, aerodynamic mispredictions, and off-nominal atmospheric interface conditions.

Postaerocapture ΔV is used as a figure of merit in evaluating mission success. With the algorithm included as part of the simulation, the postaerocapture ΔV budget was shown to be insensitive to Mars-GAM-generated random atmospheric density profiles. The guidance algorithm was able to tolerate mispredictions in the vertical atmospheric density profile, errors in aerodynamics, and errors at the atmospheric interface with only a small increase in postaerocapture ΔV even when the errors are simulated simultaneously (less than 22 m/s at an atmospheric interface velocity of 6 km/s and less than 47 for an atmospheric interface velocity of 8 km/s). However, horizontal density waves at short wavelengths (e.g., 50 km) did result in a relatively large postaerocapture ΔV (although it was still within reasonable margins). The required ΔV for these horizontal wave cases could be reduced by the addition of density filtering.

Overall, this study demonstrated that the addition of vehicle dynamics to the Mars aerobraking simulation does not significantly impact mission feasibility. That is, a good control system design coupled with an adaptive guidance algorithm can ensure mission success (as measured by the required postaerocapture propulsive maneuvers) in the presence of atmospheric density uncertainties, off-nominal atmospheric interface conditions, and vehicle aerodynamic characteristics mispredictions.

Acknowledgment

The authors are indebted to M. Fouché of Boeing Aerospace in Huntsville, Alabama, for the development of the horizontal wave equation used in this analysis and for several discussions pertaining to atmospheric density variations on Mars.

References

[1]Braun, R. D., Powell, R. W., and Hartung, L. C., "The Effect of Interplanetary Trajectory Options on a Manned Mars Aerobrake Configuration," NASA TP-3019, Aug. 1990.

[2]Fuhry, D. P., "A Design Study of Onboard Navigation and Guidance During Aerocapture at Mars," M.S. Thesis, Massachusetts Inst. of Technology, Cambridge, MA, May 1988.

[3]Willcockson, W. H., "Mars Aerocapture Using Continuous Roll Techniques," American Astronautical Society Paper 91-422, Aug. 1991.

[4]Shipley, B. W., and Ward, D. T., "Control Algorithms for Aerobraking in the Martian Atmosphere," American Astronautical Society Paper 91-120, Feb. 1991.

[5]Spratlin, K. M., "An Adaptive Numeric Predictor-Corrector Guidance Algorithm for Atmospheric Entry Vehicles," M.S. Thesis, Massachusetts Inst. of Technology, Cambridge, MA, May 1987.

[6]AviDyne, K., "Guidance and Navigation for Entry Vehicles," NASA SP-8015, Nov. 1968.

[7]Gamble, J. D., Cerimele, C. J., Moore, T. E., and Higgins, J., "Atmospheric Guidance Concepts for an Aeroassist Flight Experiment," *Journal of Astronautical Sciences,* Vol. 36, No. 1/2, Jan.–June 1988, pp. 45–71.

[8]Braun, R. D., and Powell, R. W., "A Predictor-Corrector Guidance Algorithm for Use in High-Energy Aerobraking System Studies," *Journal of Guidance, Control, and Dynamics,* Vol. 15, No. 3, 1992, pp. 672–678.

[9]Striepe, S. A., Braun, R. D., and Powell, R.W., "Interplanetary Trajectory Optimization of Mars Aerobrake Missions with Constrained Atmospheric Entry Velocities," American Astronautical Society Paper 91-421, Aug. 1991.

[10]Cheatwood, F. M., DeJarnette, F. R., and Hamilton, H. H., II, "Geometrical Description for a Proposed Aeroassist Flight Experiment Vehicle," NASA TM-87714, 1986.

[11]Wells, W. L., "Measured and Predicted Aerodynamic Coefficients and Shock Shapes for Aeroassist Flight Experiment Configuration," NASA TP-2956, Jan. 1990.

[12]Freeman, D. C., Jr., and Powell, R. W., "Manned Mars Aerobrake Vehicle Design Issues," *Space Technology Industrial and Commercial Applications,* Vol. 12, No. 3, July 1992, pp. 313–324.

[13]Mahesh, J. K., Konar, A. F., and Ward, M. D., "Interactive Flight Control System Analysis Program," NASA CR-172352, June 1984.

[14]Brauer, G. L., Cornick, D. E., and Stevenson, R., "Capabilities and Applications of the Program to Optimize Simulated Trajectories (POST)," NASA CR-2770, Feb. 1977.

[15]Justus, C., "A Mars Global Reference Atmospheric Model (Mars-GRAM) for Mission Planning and Analysis," AIAA Paper 90-0004, Jan. 1990.

[16]Konopliv, A., and Wood, L., "High Accuracy Mars Approach Navigation with Radiometric and Optical Data," AIAA Paper 90-2907, Aug. 1990.